

## MIT Open Access Articles

*Photochemical Generation of a Tryptophan Radical  
within the Subunit Interface of Ribonucleotide Reductase*

The MIT Faculty has made this article openly available. **Please share**  
how this access benefits you. Your story matters.

**Citation:** Olshansky, Lisa; Greene, Brandon L.; Finkbeiner, Chelsea; Stubbe, JoAnne and Nocera, Daniel G. "Photochemical Generation of a Tryptophan Radical Within the Subunit Interface of Ribonucleotide Reductase." *Biochemistry* 55, no. 23 (June 2016): 3234–3240 © 2016 American Chemical Society

**As Published:** <http://dx.doi.org/10.1021/acs.biochem.6b00292>

**Publisher:** American Chemical Society (ACS)

**Persistent URL:** <http://hdl.handle.net/1721.1/109908>

**Version:** Author's final manuscript: final author's manuscript post peer review, without publisher's formatting or copy editing

**Terms of Use:** Article is made available in accordance with the publisher's policy and may be subject to US copyright law. Please refer to the publisher's site for terms of use.





Published in final edited form as:

Biochemistry. 2016 June 14; 55(23): 3234–3240. doi:10.1021/acs.biochem.6b00292.

## Photochemical Generation of a Tryptophan Radical within the Subunit Interface of Ribonucleotide Reductase

Lisa Olshansky<sup>a,b</sup>, Brandon L. Greene<sup>a</sup>, Chelsea Finkbeiner<sup>b</sup>, JoAnne Stubbe<sup>b</sup>, and Daniel G. Nocera<sup>a</sup>

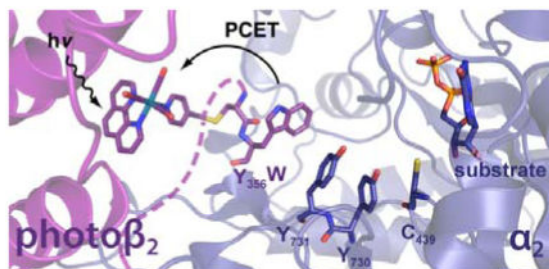
<sup>a</sup> Department of Chemistry and Chemical Biology, 12 Oxford Street, Cambridge, MA 02138–2902; dnocera@fas.harvard.edu

<sup>b</sup> Department of Chemistry, Massachusetts Institute of Technology, 77 Massachusetts Avenue, Cambridge, MA 02139-4307; stubbe@mit.edu.

### Abstract

The *E. coli* class Ia ribonucleotide reductase (RNR) achieves forward and reverse proton-coupled electron transfer (PCET) over a pathway of redox-active amino acids ( $\beta$ -Y<sub>122</sub>  $\rightleftharpoons$   $\beta$ -Y<sub>356</sub>  $\rightleftharpoons$   $\alpha$ -Y<sub>731</sub>  $\rightleftharpoons$   $\alpha$ -Y<sub>730</sub>  $\rightleftharpoons$   $\alpha$ -C<sub>439</sub>) spanning  $\sim 35$  Å and two subunits every time it turns over. We have developed photoRNRs that allow radical transport to be phototriggered at tyrosine (Y) or fluorotyrosine (F<sub>n</sub>Y) residues along the PCET pathway. We now report a new photoRNR in which photooxidation of a tryptophan (W) residue replacing Y<sub>356</sub> within the  $\alpha/\beta$  subunit interface proceeds by a stepwise ETPT (electron transfer then proton transfer) mechanism and provides an orthogonal spectroscopic handle with respect to radical pathway residues Y<sub>731</sub>/Y<sub>730</sub> in  $\alpha$ . This construct displays a  $\sim 3$ -fold enhancement in photochemical yield of W• relative to F<sub>3</sub>Y• and a  $\sim 7$ -fold enhancement relative to Y•. Photogeneration of the W• radical occurs with a rate constant of  $4.4 \pm 0.2 \times 10^5 \text{ s}^{-1}$ , which obeys a Marcus correlation for radical generation at the RNR subunit interface. Despite the fact that the Y  $\rightarrow$  W variant displays no enzymatic activity in the absence of light, photogeneration of W• within the subunit interface results in 20% activity for turnover relative to wt-RNR under the same conditions.

### Abstract



Supporting Information

Supporting information available including a detailed materials and methods description and emission lifetime traces.

Ribonucleotide reductase (RNR) catalyzes the conversion of nucleotides to deoxynucleotides in all organisms, providing the monomeric building blocks for DNA replication and repair. The class Ia RNR from *E. coli* is composed of two homodimeric subunits,  $\alpha_2$  which contains the active site and  $\beta_2$  which houses the  $\text{Fe}^{\text{III}}_2(\mu\text{-O})/\text{Y}_{122}^\bullet$  cofactor required to initiate active site radical chemistry.<sup>1</sup> The active oligomeric state is an  $\alpha_2\beta_2$  complex<sup>2-4</sup> that comes together transiently during turnover to accomplish long-range ( $\sim 35$  Å) radical translocation over a pathway of redox active amino acids ( $\beta\text{-Y}_{122} \rightleftharpoons \beta\text{-Y}_{356} \rightleftharpoons \alpha\text{-Y}_{731} \rightleftharpoons \alpha\text{-Y}_{730} \rightleftharpoons \alpha\text{-C}_{439}$ ) via a series of individual proton-coupled electron transfer (PCET) hopping steps.<sup>5,6</sup>

Pre-steady state kinetics of RNR turnover reveal that the rate-determining step in this mechanism is a conformational change triggered by substrate binding that occurs at 2–10 s<sup>-1</sup>.<sup>7</sup> In order to study the kinetics of individual PCET steps during turnover, we have developed methods to initiate radical transport within RNR photochemically.<sup>8-10</sup> Installation of a bromomethylpyridyl rhenium(I) tricarbonyl phenanthroline complex ( $[\text{Re}^{\text{I}}]$ ) at position  $\beta_{355}$  via cysteine ligation produces a photo $\beta_2$ ,<sup>11</sup> where the adjacent  $\text{Y}_{356}$  has been replaced with various fluorotyrosines ( $\text{F}_n\text{Ys}$ ,  $n = 2-3$ ) to modulate the  $\text{p}K_a$  and  $E^\circ$  of  $\text{Y}_{356}$  within the RNR subunit interface.<sup>12,13</sup> This methodology has enabled spectroscopic observation of photochemically competent radical intermediates,<sup>9,12</sup> assignment of rate constants associated with individual PCET steps,<sup>12</sup> and determination of Marcus parameters within the  $\alpha/\beta$  subunit interface.<sup>13</sup> In these studies, individual  $\text{Y}^\bullet$  species from among the  $\beta\text{-Y}_{356}$ ,  $\alpha\text{-Y}_{731}$  and  $\alpha\text{-Y}_{730}$  triad could not be spectroscopically resolved, preventing measurement of PCET rates among them. In one approach toward unraveling the PCET kinetics associated with the tyrosine triad, a  $\text{Y}_{356}\text{W}$ -photo $\beta_2$  construct has been prepared. We show that photoinitiation of  $\text{Y}_{356}\text{W}$ -photo $\beta_2$  yields a  $\bullet\text{W}_{356}$  radical absorption feature that is well-resolved from that of  $\text{Y}^\bullet$ . With this  $\text{Y}_{356}\text{W}$ -photo $\beta_2$ , we have begun to disentangle individual PCET kinetics among the  $\beta\text{-Y}_{356} \rightleftharpoons \alpha\text{-Y}_{731} \rightleftharpoons \alpha\text{-Y}_{730}$  triad of RNR. We show that the rate for radical generation within the amino acid triad is described well by a Marcus treatment of charge transport.

## Materials and Methods

Wt- $\alpha_2$  (2,000 nmol/mg/min) and  $\text{Y}_{731}\text{F-}\alpha_2$  were expressed and purified as previously described.<sup>14</sup> All  $\alpha_2$  proteins were pre-reduced prior to use by incubation with 30 mM DTT for 30 min at RT followed by buffer exchange.  $[5\text{-}^3\text{H}]\text{-cytidine } 5'\text{-diphosphate sodium salt hydrate}$  ( $[5\text{-}^3\text{H}]\text{-CDP}$ ) was purchased from ViTrax (Placentia, CA), Tricarbonyl(1,10-phenanthroline)(4-bromomethyl-pyridine)rhenium(I) hexafluorophosphate ( $[\text{Re}^{\text{I}}]\text{-Br}$ ) was available from a previous study.<sup>11</sup> *E. coli* thioredoxin (TR, 40  $\mu\text{mol/min/mg}$ ) and thioredoxin reductase (TRR, 1,800  $\mu\text{mol/min/mg}$ ) were prepared as previously described.<sup>15,16</sup>  $\text{C}_{268}\text{S/C}_{305}\text{S/S}_{355}\text{C/Y}_{356}\text{W-}\beta_2$  and  $\text{Y}_{356}\text{W-}\beta_2$  were generated by site-directed mutagenesis using the primers described in the SI, and expressed and purified as previously reported for related photo $\beta_2$  variants.<sup>12</sup> All photo $\beta_2$ s were reduced with hydroxyurea prior to measurements to eliminate the native tyrosyl radical cofactor.  $\text{C}_{268}\text{S/C}_{305}\text{S/S}_{355}\text{C/Y}_{356}\text{F-}\beta_2$  was available from a previous study.<sup>12</sup> Assay buffer consists of 50 mM HEPES, 15 mM  $\text{MgSO}_4$  and 1 mM EDTA adjusted to pH 7.6.

Photochemical turnover experiments were performed as previously reported under two conditions, those similar to TA spectroscopy (in the presence of 10 mM Ru(NH<sub>3</sub>)<sub>6</sub>Cl<sub>3</sub>), and those similar to emission quenching measurements (in the absence of Ru(NH<sub>3</sub>)<sub>6</sub>Cl<sub>3</sub>).<sup>12</sup> In each case, 10 μM of either Y<sub>356</sub>W- or Y<sub>356</sub>F-photoβ<sub>2</sub> was mixed with either wt- or Y<sub>731</sub>F-α<sub>2</sub> (10 μM), 0.2 mM [5-<sup>3</sup>H]-CDP (specific activity 26,700 cpm/nmol), 1 mM ATP, and with or without 10 mM Ru(NH<sub>3</sub>)<sub>6</sub>Cl<sub>3</sub> in assay buffer at pH 7.6. Samples were placed in a 4 mm × 4 mm quartz cuvette and held at 25 °C under illumination for 10 min with white light powered at 800 W (35 V and 24 A DC) in conjunction with a 313 nm long-pass cutoff filter. Quantitation of radioactive products by scintillation counting was performed as previously described.<sup>10,12,17</sup> The data presented are averages of 3 independently prepared samples, and error bars represent one standard deviation (s.d.).

Nanosecond spectroscopy was performed using a modified version of a previously reported home-built Nd:YAG laser system.<sup>9</sup> In the modified setup, the previously used Triax 320 spectrometer has been replaced by a Horiba iHR320 spectrometer. Optical long-pass cutoff filters (λ > 375 nm) were used to filter probe light before detection to remove scattered 355 nm pump light. The reported experiments used a 250 nm blaze grating (300 grooves/mm). The power of the pump beam (λ = 355 nm) was set to 2 mJ/pulse.

For transient absorption (TA) spectra, the output of the Xe-arc lamp was set to 3.0 ms pulses with 30 A current. TA spectra and kinetic traces are the averages of measurements made from 1000 laser shots (500 four spectrum sequences in the case of the TA spectra) on 3 independently prepared samples. TA samples were prepared in a total volume of 650 μL and recirculated through a 1 cm path length flow-cell to reduce sample decomposition. An inline filter (Acrodisc 13 mm 0.2 μM Supor Membrane, Pall Corporation) was used to collect solid photoproducts. Samples contained either 50 μM Y<sub>356</sub>W-photoβ<sub>2</sub> with and without 75 μM wt-α<sub>2</sub>, or 30 μM Y<sub>356</sub>F-photoβ<sub>2</sub> with and without 50 μM wt-α<sub>2</sub>, and 1 mM CDP, 3 mM ATP and 10 mM Ru(NH<sub>3</sub>)<sub>6</sub>Cl<sub>3</sub> in assay buffer at pH 7.6. Single wavelength kinetics data were collected at 520 or 560 nm using slit widths corresponding to ±1 nm resolution and least-squares fitting was performed using the OriginPro 8.0 data analysis software over 3–80 μs according to Eq. 1, accounting for the instrument response and radical decay.

$$y=y_0+A_1e^{-\tau/t_1}+A_2e^{-\tau/t_2} \quad (1)$$

Emission quenching experiments were prepared in a total volume of 550 μL and recirculated through a 1 cm path length flow-cell to reduce sample decomposition. Samples contained 10 μM Y<sub>356</sub>W- or Y<sub>356</sub>F-photoβ<sub>2</sub>, 1 mM CDP, 3 mM ATP, with or without 25 μM wt- or Y<sub>731</sub>F-α<sub>2</sub>, in assay buffer at pH 7.6. Single wavelength kinetics data were collected at 600 nm using slit widths corresponding to ±0.75 nm resolution and recorded over 1000 laser shots for each sample. Lifetime data were obtained in triplicate with independently prepared samples for each experimental condition and least-squares fitting were performed using the OriginPro 8.0 data analysis software over the 0.1–4.5 μs time window according to Eq. 2.

$$y = y_0 + A_1 e^{-\tau/t} \quad (2)$$

Triplicate measurements were performed in all cases and error associated with the goodness of fit, as well as that between replicates, was propagated. Calculation of  $k_q$  is achieved by applying Eq. 3, where the inverse of the excited state lifetimes measured in the presence of Y<sub>356</sub>W- and Y<sub>356</sub>F-photoβ<sub>2</sub>s ( $\tau_W$  and  $\tau_F$ , respectively) are subtracted. Eq. 4 was used to propagate error, where  $\sigma_W$  and  $\sigma_F$  are the standard deviations for the triplicate measurements of each (compounded with error associated with the goodness of fit), and  $\delta$  is the final reported error  $k_q$ .

$$k_q = \frac{1}{\tau_W} - \frac{1}{\tau_F} \quad (3)$$

$$\delta = \sqrt{\left(\frac{\sigma_W}{\tau_W^2}\right)^2 + \left(\frac{\sigma_F}{\tau_F^2}\right)^2} \quad (4)$$

## Results

### Preparation and characterization of Y<sub>356</sub>W-photoβ<sub>2</sub>

Photoβ<sub>2</sub>s are prepared by replacing two surface cysteine residues (C<sub>268</sub> and C<sub>305</sub>) with serines, and by replacing a single surface serine (S<sub>355</sub>) with cysteine. This allows site-specific conjugation of a [Re<sup>I</sup>] photooxidant at position 355 by performing an S<sub>N</sub>2 reaction with [Re<sup>I</sup>(CO)<sub>3</sub>(phen)(PyCH<sub>2</sub>Br)]PF<sub>6</sub>. Here, we have also replaced the adjacent redox-active Y<sub>356</sub> residue with W. Neither the unlabelled (S<sub>355</sub>C-Y<sub>356</sub>W-β<sub>2</sub>) nor the labelled ([Re]<sub>355</sub>-Y<sub>356</sub>W-photoβ<sub>2</sub>) constructs exhibit enzymatic activity under steady-state turnover conditions performed in the dark (RNR assay conditions are described in the SI). Measurement of the  $K_d$  for the Y<sub>356</sub>W-photoβ<sub>2</sub>:α<sub>2</sub> interaction was performed by a competitive inhibition assay shown in Figure 1. The value of  $K_d = 0.8 \pm 0.1 \mu\text{M}$  obtained is only slightly larger than that of the wt-α<sub>2</sub>:β<sub>2</sub> (0.2 μM)<sup>18</sup> and essentially equal to the  $K_d = 0.7 \pm 0.1 \mu\text{M}$  measured for the Y-photoβ<sub>2</sub>:α<sub>2</sub> interaction.<sup>10</sup>

### Photochemistry

Photooxidation of W<sub>356</sub> can be achieved by two methods schematically represented in Figure 2. Direct excitation ( $\lambda_{\text{exc}} = 355 \text{ nm}$ ) of [Re<sup>I</sup>] gives rise to a <sup>3</sup>[Re<sup>I</sup>]\* excited state (after intersystem crossing from the initially formed singlet state), which is sufficiently oxidizing and long-lived to directly oxidize an adjacent amino acid, namely W<sub>356</sub>, to produce a charge-separated state [Re<sup>0</sup>]-W•. The kinetics of this process report on the rate of formation of W• and can be assessed by monitoring the emission lifetime of <sup>3</sup>[Re<sup>I</sup>]\*. An additional method for photooxidizing W<sub>356</sub> is by generating <sup>3</sup>[Re<sup>I</sup>]\* in the presence of a large excess of

Ru(NH<sub>3</sub>)Cl<sub>3</sub>, which functions as a “flash-quencher”. In this case, Ru(NH<sub>3</sub>)Cl<sub>3</sub> oxidatively quenches <sup>3</sup>[Re<sup>I</sup>]\* to [Re<sup>II</sup>]; the resultant [Re<sup>II</sup>] is a potent oxidant ( $E^{\circ'} = 2.07$  V, *vide infra*, Figure 2c)<sup>19</sup> capable of oxidizing W<sub>356</sub> to yield a •W–[Re<sup>I</sup>] state. The kinetics of W• (and/or WH•<sup>+</sup>) formation and decay are monitored by transient absorption spectroscopy. The two methods differ primarily in their ability to undergo the reverse reaction, charge-recombination. In the former case, charge recombination within the photochemically generated •W–[Re<sup>0</sup>] generates the initial W–[Re<sup>I</sup>] state. The rate constant with which •W–[Re<sup>0</sup>] is produced by charge-separation, is similar to that with which it returns to W–[Re<sup>I</sup>] by charge recombination, thus lowering the yield of the photogenerated radical for spectroscopic analysis. This experimental hurdle is circumvented by using the Ru(NH<sub>3</sub>)Cl<sub>3</sub> as there is no charge-recombination pathway available with the elimination of [Re<sup>0</sup>] upon its reaction with the external Ru<sup>III</sup> flash quencher. The net result is that the photochemical yield of W• (and/or WH•<sup>+</sup>) is increased, this allowing for the direct observation of spectroscopic signals associated with the radical species.

W and Y amino acids are among the most ubiquitous in facilitating biological ET reactions.<sup>20</sup> In comparing the two, Y is much more likely to undergo a concerted PCET (CPET) reaction<sup>21</sup> due to the extremely acidic nature of the YH•<sup>+</sup> moiety ( $pK_a \approx -2$ <sup>22</sup>). On the contrary, WH•<sup>+</sup> has a much higher  $pK_a$  ( $\approx +4.5$ )<sup>23</sup> making a stepwise ETPT process also possible at physiological pH. Figure 3 shows the TA spectrum of Y<sub>356</sub>W-photoβ<sub>2</sub>:α<sub>2</sub> (blue circles) collected 8 μs after excitation under flash quench conditions. The TA spectrum of the control Y<sub>356</sub>F-photoβ<sub>2</sub>:α<sub>2</sub> (black circles) was also examined. Here the control Y<sub>356</sub>F-photoβ<sub>2</sub> serves as a measure of the non-specific photochemical W oxidation, as there are additional W residues within β<sub>2</sub>. The λ<sub>max</sub> observed at 520 nm for the Y<sub>356</sub>W-photoβ<sub>2</sub>:α<sub>2</sub> complex (and for Y<sub>356</sub>W-photoβ<sub>2</sub>, Figure S1) are consistent with the deprotonated W• radical rather than a protonated radical cation (WH•<sup>+</sup>), which typically display an absorption maximum at ~560-580 nm.<sup>24</sup> We do not observe the formation of any significant amount of a WH•<sup>+</sup> intermediate over the time course (3–20 μs) of radical decay. The sharp absorption feature at 410 nm in Figure 3 is consistent with that of Y•.<sup>12,25,26</sup> Given typical extinction coefficients observed for W• (~2,000 M<sup>-1</sup> cm<sup>-1</sup>)<sup>24</sup> and Y• (~3,000 M<sup>-1</sup> cm<sup>-1</sup>)<sup>25</sup> within various enzymes,<sup>1</sup> the OD of  $3.3 \times 10^{-3}$  that we observe in the flash-quenched Y<sub>356</sub>W-photoβ<sub>2</sub>:α<sub>2</sub> complex represents a 3- and 7-fold enhancement in the yield of photogenerated radical relative to the 2,3,5-F<sub>3</sub>Y- and Y-photoβ<sub>2</sub>s respectively.<sup>10,12</sup> When W is replaced by a redox inert F, signatures consistent with W• were also observed but with significantly different spectral character. The flash-quenched Y<sub>356</sub>F-photoβ<sub>2</sub>:α<sub>2</sub> construct exhibits a spectrum with a broad signal at λ<sub>max</sub> ~ 530 nm and a small shoulder at 590 nm (Figure 3, black circles). Additional controls in which the TA spectra of Y<sub>356</sub>W-photoβ<sub>2</sub> and Y<sub>356</sub>F-photoβ<sub>2</sub> were measured in the absence of α<sub>2</sub> are shown in Figure S1. In the absence of α<sub>2</sub>, the λ<sub>max</sub> associated with W• was red-shifted to 570 nm, consistent with WH•<sup>+</sup>. These results suggest multiple distinct W oxidation processes which may evolve differently, and appear distinct from the spectrum of the Y<sub>356</sub>W-photoβ<sub>2</sub>:α<sub>2</sub>. Another small peak at 410 nm was also observed in the transient spectra of the Y<sub>356</sub>F-photoβ<sub>2</sub> consistent with a small amount of tyrosine oxidation within β<sub>2</sub> (Figure S1).



## Photochemical turnover

In the presence of wt- $\alpha_2$ , substrate (CDP) and effector (ATP), illumination of Y<sub>356</sub>W-photo $\beta_2$  results in dCDP formation. Here, the total number of dCDP produced is limited by the amount of  $\alpha_2$  present. Re-reduction of the four participating cysteine residues in  $\alpha_2$  is required for additional turnovers. Typically these reducing equivalents are supplied by coupled reactions with thioredoxin, thioredoxin reductase, and NADPH. In the absence of such a reducing system a “single turnover” gives a theoretical maximum of 4 dCDP/ $\alpha_2$ . Figure 4 shows the results of photochemically driven single turnovers, both in the presence and absence of flash quencher. Greater turnover numbers (20% relative to wt- $\beta_2$  under the same conditions) are observed with the Ru(NH<sub>3</sub>)<sub>6</sub><sup>3+</sup> flash-quench reagent (burgundy bar), presumably owing to the longer lifetime of the oxidatively quenched state as compared to using the excited state (purple bar) as the oxidant (4% turnover relative to wt- $\beta_2$  under the same conditions). We note that the wt experiments were performed with a  $\beta_2$  that retains the native Y• cofactor (has not been reduced with HU) and lacks a [Re<sup>I</sup>] photosensitizer, thus representing a single turnover experiment performed under the conditions of the photochemical experiments. No turnover is observed for the Y<sub>356</sub>W-photo $\beta_2$ : $\alpha_2$  complex in the dark (blue bar) or if a radical block is placed in the PCET pathway (Y → F at position 356 in  $\beta$  or 731 in  $\alpha$ ). This observation is consistent with the distinction between the spectral signatures of Y<sub>356</sub>W- and Y<sub>356</sub>F-photo $\beta_2$  constructs (Figure 3). Of the five photo $\beta_2$  constructs previously reported (Y-, 3,5-F<sub>2</sub>Y-, 2,3-F<sub>2</sub>Y-, 2,3,5-F<sub>3</sub>Y- and 2,3,6-F<sub>3</sub>Y-photo $\beta_2$ ), the Y<sub>356</sub>W-photo $\beta_2$  variant displays photochemical turnover activity second only to that in which the native Y residue is retained at position 356.<sup>13</sup> As noted previously, the  $K_{Ds}$  for Y- and Y<sub>356</sub>W-photo $\beta_2$  constructs are similar. Thus, the slightly decreased activity of Y<sub>356</sub>W-photo $\beta_2$  relative to Y-photo $\beta_2$  is not a function of weaker binding affinity for the  $\alpha_2$  subunit.

## PCET Kinetics

The single wavelength kinetics decay curve of the photogenerated W• as probed by TA spectroscopy is shown in Figure 5. Formation of W• monitored at 520 nm could not be observed directly by TA spectroscopy due to spectral and temporal overlap with the <sup>3</sup>[Re<sup>I</sup>]\* emission ( $\lambda_{max} \sim 540$  nm), even under flash-quench conditions. To address this, we examined the quenching kinetics of the <sup>3</sup>[Re<sup>I</sup>]\* excited state in the presence of W by time-resolved emission spectroscopy (Table 1). To calculate the quenching rate constant, we measured the <sup>3</sup>[Re<sup>I</sup>]\* excited state lifetime in Y<sub>356</sub>W-photo $\beta_2$  ( $\tau_W$ ) and Y<sub>356</sub>F-photo $\beta_2$  ( $\tau_F$ ). Substituting these lifetime values into Eq. 3 furnishes the rate constant of  $k_q = 4.4 \pm 0.2 \times 10^5$  s<sup>-1</sup> for the quenching of <sup>3</sup>[Re<sup>I</sup>]\* by W oxidation in the presence of wt- $\alpha_2$ .

The W• radical observed in the TA spectrum of Y<sub>356</sub>W-photo $\beta_2$ : $\alpha_2$  decays with a rate constant of  $4.4 \pm 0.2 \times 10^4$  s<sup>-1</sup> (Figure 5). This rate constant is in-line with our previous observations using other photo $\beta_2$ s in the presence of wt- $\alpha_2$ .<sup>12</sup> Unlike Y- and F<sub>3</sub>Y-photo $\beta_2$ s, neither the absence of wt- $\alpha_2$ , nor the presence of Y<sub>731</sub>F-, 3,5-F<sub>2</sub>Y<sub>731</sub>- or 2,3,5-F<sub>3</sub>Y<sub>731</sub>- $\alpha_2$  result in significant changes in these kinetics. In the case of the Y<sub>356</sub>W-photo $\beta_2$ , disruption of the PCET pathway is apparent from comparing the data in the top and bottom halves of Table 1; there is no enhancement in  $k_q$  measured in the presence of wt- versus Y<sub>731</sub>F- $\alpha_2$ . In contrast, with Y-photo $\beta_2$  a ~24% enhancement in  $k_q$  for the intact PCET pathway is observed relative to the case with the pathway blocked at position  $\alpha_{731}$ .<sup>10</sup> These data suggest

that the difference in reactivity between W<sub>356</sub>-photoβ<sub>2</sub> and Y<sub>356</sub>-photoβ<sub>2</sub> result from a misalignment or disruption of the PCET pathway incurred upon replacing Y<sub>356</sub> with W.

## Discussion

The Y<sub>356</sub>W-β<sub>2</sub> construct of *E. coli* RNR has previously been shown to have no enzymatic activity, even when assayed *in vivo* by highly sensitive screening method.<sup>27</sup> We also observe that Y<sub>356</sub>W-β<sub>2</sub>, and the unlabeled-Y<sub>356</sub>W-photoβ<sub>2</sub> containing the three mutations necessary for the production of photoβ<sub>2</sub>s (C<sub>268</sub>S, C<sub>305</sub>S and S<sub>355</sub>C), are inactive. The only activity observed arises from low amounts of endogenous wt-β<sub>2</sub> present as a result of the fact that RNR is an essential enzyme. The inactivity of these Y → W-β<sub>2</sub> variants may result simply from perturbation of the β<sub>356</sub> reduction potential, since progressively lower activity is measured for RNRs with F<sub>n</sub>Ys incorporated at position β-356 as the  $E^{\circ}(\text{F}_n\text{Y}\bullet/\text{F}_n\text{Y}-)$  approach that of  $E^{\circ}(\text{WH}\bullet^{+}/\text{WH})$ .<sup>28</sup> Another explanation for the observed inactivity may be due to a misalignment of the PCET pathway. We have shown that this inactivity may be overcome by photogeneration of W•. As shown in Figure 4, Y<sub>356</sub>W-photoβ<sub>2</sub> is active for turnover under illumination. The photochemical system possesses significant overpotential for W• generation and hence the barriers to the generation of a •W<sub>356</sub> are overcome and forward radical propagation into α<sub>2</sub> becomes possible in the photo RNR.

The two methods employed to photogenerate the W• radical are schematically described in Figure 2. The W• radical may be photogenerated by direct oxidation from the triplet excited state of the [Re] complex (<sup>3</sup>[Re<sup>I</sup>]\*) (Figure 2a) or by oxidation from the [Re<sup>II</sup>] complex, produced by the flash-quench method (Figure 2b). The energetics associated with the [Re] complex of the two different pathways is summarized in Figure 2c. The rate constant for W oxidation, as measured by emission quenching, of  $4.4 \pm 0.2 \times 10^5 \text{ s}^{-1}$ , is very similar to that of Y• or F<sub>n</sub>Y• formation,<sup>10,12</sup> despite their significant differences in  $G^{\circ}$ .

The rate constant for W oxidation is consistent with an ET process, as opposed to a PCET process, and accordingly follows a Marcus formalism described in equation Eq. 5,

$$k_{ET} = \frac{2\pi H_{DA}^2}{\hbar \sqrt{4\pi\lambda k_B T}} \cdot e^{-\frac{(\lambda + \Delta G^{\circ})^2}{4\lambda k_B T}} \quad (5)$$

Figure 6 plots the previously measured rate constants for radical formation in a series of F<sub>n</sub>Y-photoβ<sub>2</sub>s (n = 0–3) within the photoRNR complex. Over the pH regime examined, the F<sub>n</sub>Ys are deprotonated and radical generation in β-F<sub>n</sub>Y<sub>356</sub> occurs by ET. Moreover, the PCET process for Y oxidation in the presence of α<sub>2</sub> also behaves kinetically like an ET process owing to fast proton transfer from the interface. As is clearly evident from the Marcus plot, the ET process for radical generation within the F<sub>n</sub>Y-photoβ<sub>2</sub>:α<sub>2</sub> complex occurs in the Marcus inverted regime, where an increase in  $|\Delta G^{\circ}|$  results in a decrease in  $k_q$ .<sup>13</sup> The F<sub>n</sub>Y-photoβ<sub>2</sub> series has now been expanded to include  $k_q$  measured for the Y<sub>356</sub>W-photoβ<sub>2</sub>:α<sub>2</sub> complex, assuming similar  $H_{DA}$  and  $\lambda$  parameters between the mutations. Based on the  $E^{\circ}$  of 1.15 V (vs NHE) for WH•<sup>+</sup> + e<sup>-</sup> → WH measured by differential pulse voltammetry,<sup>29</sup> and an excited state reduction potential for [Re<sup>I</sup>]\* → [Re<sup>0</sup>] of 1.94 V vs



NHE (Figure 2c),<sup>13</sup> we calculate the  $-G^\circ$  for W oxidation of 0.79 V. At this potential, the measured rate constant from the  $[\text{Re}^{\text{I}}]^*$  quenching experiment of  $4.4 \pm 0.2 \times 10^5 \text{ s}^{-1}$  falls on the Marcus curve in Figure 6. This result indicates that tryptophan oxidation proceeds by ET to furnish  $\text{WH}^{\bullet+}$ . We note, however, that the TA spectrum of Figure 3 is that of  $\text{W}^\bullet$  as opposed to  $\text{WH}^{\bullet+}$ . Together, the quenching and TA kinetics indicate an ET/PT process in which rate-limiting ET precedes rapid proton loss to produce  $\text{W}^\bullet$ . The fast proton loss is consistent with the  $\text{p}K_{\text{a}}$  of 3.1 between  $\text{WH}^{\bullet+}$  and bulk solution ( $\text{pH} = 7.6$ ).

Finally, a reorganization energy of  $\lambda = 1 \text{ eV}$  is determined for the ET process at the photoRNR  $\alpha_2/\beta_2$  interface. This value is 0.9 eV lower than that determined for  $[\text{Re}^{\text{I}}]\text{-F}_n\text{Y}$  model complexes in solution,<sup>30</sup> revealing that the enzyme microenvironment exerts a significant influence in minimizing the reorganization energy. Similar reductions in the reorganization energy have been observed for Cu enzymes as compared to Cu metal complexes,<sup>31</sup> and more generally for a host of metallocofactors embedded within protein matrices.<sup>32</sup>

## Conclusions

W and Y are among the most common amino acids to facilitate biological ET reactions.<sup>1,22</sup> In comparing the two, Y is much more likely to undergo a concerted PCET (CPET) reaction due to the extremely acidic nature of the  $\text{YH}^{\bullet+}$  moiety ( $\text{p}K_{\text{a}} \approx -2$ ). The much higher  $\text{p}K_{\text{a}}$  of  $\text{WH}^{\bullet+}$  ( $\approx +4.5$ ) makes a stepwise ET/PT process possible at physiological pH as we observe here. A concerted PCET mechanism has been proposed in rare instances for model complexes,<sup>33</sup> but to our knowledge this has not been observed in a biological system. The formation of  $\text{W}^\bullet$  at  $\beta_{356}$  obeys a Marcus formalism indicating that  $\text{W}_{356}\text{-photo}\beta_2$  oxidation proceeds through  $\text{WH}^{\bullet+}$ . The appearance of  $\text{W}^\bullet$  in the TA spectrum points to fast proton loss, indicating an ET/PT mechanism for radical generation in the  $\text{Y}_{356}\text{W-photo}\beta_2:\alpha_2$  complex. Conversely, radical generation in  $\text{Y}_{356}\text{-photo}\beta_2$  proceeds by a concerted PCET process, facilitated by protein-mediated PT.<sup>13</sup> Radical generation in  $\text{Y}_{356}$ - and  $\text{W-photo}\beta_2$  are also distinguished by their dependence of the PCET pathway. Photogeneration of  $\text{W}^\bullet$  is insensitive to radical blocks within the PCET pathway whereas  $\text{Y}^\bullet$  photogeneration is attenuated by the presence of the radical block. Together, these results indicate that the PCET events required for the formation of an amino acid radical at  $\beta_{356}$  are precisely controlled within the RNR protein-protein interface.

## Supplementary Material

Refer to Web version on PubMed Central for supplementary material.

## Acknowledgements

LO acknowledges the National Science Foundation's Graduate Research Fellowship Program. This research was supported by the U.S. National Institute of Health Grant GM047274 (DGN) and GM029595 (JS).

## Abbreviations

**RNR** *E. coli* class Ia ribonucleotide reductase

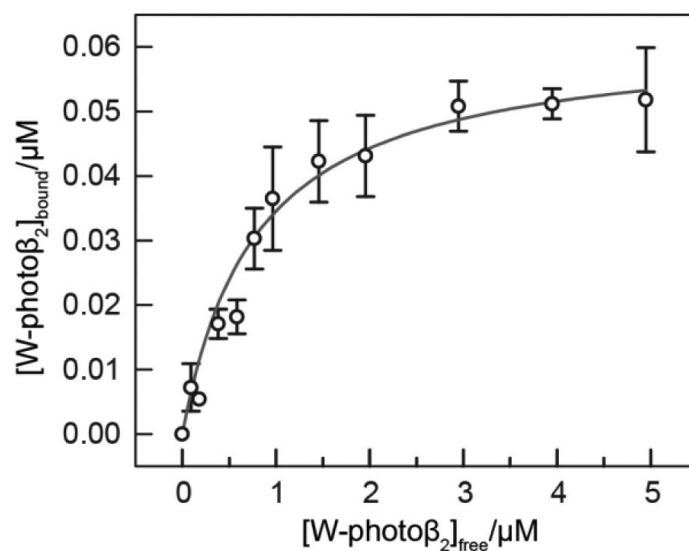
$\alpha_2$	large subunit of RNR containing substrate and effector binding sites
$\beta_2$	small subunit of RNR containing the diiron-tyrosyl radical cofactor
PCET	proton-coupled electron transfer
[Re <sup>I</sup> ]	methylpyridyl rhenium(I) tricarbonyl phenanthroline phosphorus hexafluoride complex
photo $\beta_2$	C <sub>268</sub> S/C <sub>305</sub> S/S <sub>355</sub> C- $\beta_2$ appended with [Re <sup>I</sup> ]
W-photo $\beta_2$	C <sub>268</sub> S/C <sub>305</sub> S/S <sub>355</sub> C/Y <sub>356</sub> W- $\beta_2$ appended with the [Re <sup>I</sup> ] complex
TA	transient absorption
MALDI-TOF	matrix-assisted laser desorption/ionization-time of flight
MLCT	metal-to-ligand charge transfer
HU	hydroxyurea
ATP	adenosine 5'-triphosphate
CDP	cytidine 5'-diphosphate
[ <sup>3</sup> H]-CDP	5-tritiated cytidine 5'-diphosphate sodium salt hydrate
HEPES	4-(2-hydroxyethyl)-piperazin-1-ylethanesulphonic acid
TR	thioredoxin
TRR	thioredoxin reductase
AP	calf alkaline phosphatase

## References

- (1). Stubbe J, van der Donk WA. Protein Radicals in Enzyme Catalysis. *Chem. Rev.* 1998; 98:705–762. [PubMed: 11848913]
- (2). Brown NC, Reichard P. Role of Effector Binding of Allosteric Control of Ribonucleoside Diphosphate Reductase. *J. Mol. Biol.* 1969; 46:25–38. [PubMed: 4902211]
- (3). Uhlin U, Eklund H. Structure of Ribonucleotide Reductase Protein R1. *Nature.* 1994; 370:533–539. [PubMed: 8052308]
- (4). Bennati M, Robblee JH, Mugnaini V, Stubbe J, Freed JH, Borbat P. EPR Distance Measurements Support a Model for Long-Range Radical Initiation in *E. coli* Ribonucleotide Reductase. *J. Am. Chem. Soc.* 2005; 127:15014–15015. [PubMed: 16248626]
- (5). Stubbe J, Nocera DG, Yee CS, Chang MCY. Radical Initiation in the Class I Ribonucleotide Reductase: Long-Range Proton-Coupled Electron Transfer? *Chem. Rev.* 2003; 103:2167–2202. [PubMed: 12797828]
- (6). Minnihan EC, Nocera DG, Stubbe J. Reversible, Long-Range Radical Transfer in *E. coli* Class Ia Ribonucleotide Reductase. *Acc. Chem. Res.* 2013; 46:2524–2535. [PubMed: 23730940]
- (7). Ge J, Yu G, Ator MA, Stubbe J. Pre-Steady-State and Steady-State Kinetic Analysis of *E. coli* Class I Ribonucleotide Reductase. *Biochemistry.* 2003; 42:10071–10083. [PubMed: 12939135]

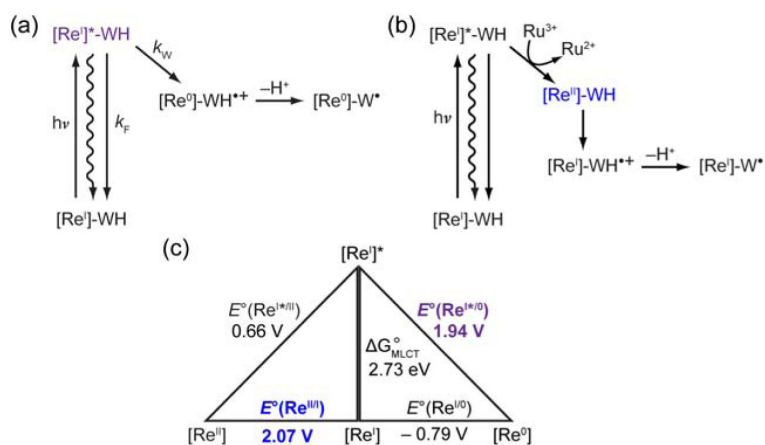
- (8). Chang MCY, Yee CS, Stubbe J, Nocera DG. Turning On Ribonucleotide Reductase by Light-Initiated Amino Acid Radical Generation. *Proc. Natl. Acad. Sci. U.S.A.* 2004; 101:6882–6887. [PubMed: 15123822]
- (9). Holder PG, Pizano AA, Anderson BL, Stubbe J, Nocera DG. Deciphering Radical Transport in the Large Subunit of Class I Ribonucleotide Reductase. *J. Am. Chem. Soc.* 2012; 134:1172–1180. [PubMed: 22121977]
- (10). Pizano AA, Olshansky L, Holder PG, Stubbe J, Nocera DG. Modulation of Y356 Photooxidation in *E. coli* Class Ia Ribonucleotide Reductase by Y731 Across the  $\alpha$ 2: $\beta$ 2 Interface. *J. Am. Chem. Soc.* 2013; 135:13250–13253. [PubMed: 23927429]
- (11). Pizano AA, Lutterman DA, Holder PG, Teets TS, Stubbe J, Nocera DG. Photo-Ribonucleotide Reductase  $\beta$ 2 by Selective Cysteine Labelling with a Radical Phototrigger. *Proc. Natl. Acad. Sci. U.S.A.* 2012; 109:39–43. [PubMed: 22171005]
- (12). Olshansky L, Pizano AA, Wei Y, Stubbe J, Nocera DG. Kinetics of Hydrogen Atom Abstraction from Substrate by an Active Site Thiyl Radical in Ribonucleotide Reductase. *J. Am. Chem. Soc.* 2014; 136:16210–16216. [PubMed: 25353063]
- (13). Olshansky L, Stubbe J, Nocera DG. Charge-Transfer Dynamics at the  $\alpha/\beta$  Subunit Interface of a Photochemical Ribonucleotide Reductase. *J. Am. Chem. Soc.* 2015; 138:1196–1205. [PubMed: 26710997]
- (14). Minnihan EC, Seyedsayamdost MR, Uhlin U, Stubbe J. Kinetics of Radical Intermediate Formation and Deoxynucleotide Production in 3-Aminotyrosine-Substituted *Escherichia coli* Ribonucleotide Reductases. *J. Am. Chem. Soc.* 2011; 133:9430–9440. [PubMed: 21612216]
- (15). Chivers PT, Prehoda KE, Volkman BF, Kim BM, Markley JL, Raines RT. Microscopic pK<sub>a</sub> Values of *Escherichia coli* Thioredoxin. *Biochemistry.* 1997; 36:14985–14991. [PubMed: 9398223]
- (16). Lunn CA, Kathju S, Wallace BJ, Kushner SR, Pigiet V. Amplification and Purification of Plasmid-encoded Thioredoxin from *Escherichia coli* K12. *J. Biol. Chem.* 1984; 259:10469–10474. [PubMed: 6381486]
- (17). Steeper JR, Steuart CD. A Rapid Assay for CDP Reductase Activity in Mammalian Cell Extracts. *Anal. Biochem.* 1970; 34:123–130. [PubMed: 5440901]
- (18). Climent I, Sjöberg B-M, Huang CY. Electron Transfer Associated with Oxygen Activation in the  $\beta$ 2 Protein of Ribonucleotide Reductase from *Escherichia coli*. *Biochemistry.* 1991; 30:5164–5171. [PubMed: 2036382]
- (19). Dattelbaum DM, Omberg KM, Schoonover JR, Martin RL, Meyer TJ. Application of Time-Resolved Infrared Spectroscopy to Electronic Structure in Metal-to-Ligand Charge-Transfer Excited States. *Inorg. Chem.* 2002; 41:6071–6079. [PubMed: 12425635]
- (20). Migliore A, Polizzi NF, Therien MJ, Beratan DN. Biochemistry and Theory of Proton-Coupled Electron Transfer. *Chem. Rev.* 2014; 114:3381–3465. [PubMed: 24684625]
- (21). Mayer JM. Proton Coupled Electron Transfer: A Reaction Chemist's View. *Annu. Rev. Phys. Chem.* 2004; 55:363–390. [PubMed: 15117257]
- (22). Harriman A. Further Comments on the Redox Potentials of Tryptophan and Tyrosine. *J. Phys. Chem.* 1987; 91:6104–6106.
- (23). Posener ML, Adams GE, Wardman P, Cundall RB. Mechanism of Tryptophan Oxidation by some Inorganic Radical-Anions: A Pulse Radiolysis Study. *J. Chem. Soc. Faraday Trans.* 1976; 1:2231–2239. 32.
- (24). Solar S, Getoff N, Surdhar PS, Armstrong DA, Singh A. Oxidation of Tryptophan and N-Methylindole by N<sub>3</sub><sup>•</sup>, Br<sub>2</sub><sup>•-</sup>, and (SCN)<sub>2</sub><sup>•-</sup> Radicals in Light- and Heavy-Water Solutions: A Pulse Radiolysis Study. *J. Phys. Chem.* 95:3639–3643.
- (25). Bansal K, Fessenden RW. Pulse Radiolysis Studies of the Oxidation of Phenols by SO<sub>4</sub><sup>•-</sup> and Br<sub>2</sub><sup>•-</sup> in Aqueous Solutions. *Radiat. Res.* 1976; 67:1–8. [PubMed: 940923]
- (26). Seyedsayamdost MR, Reece SY, Nocera DG, Stubbe J. Mono-, Di-, Tri-, and Tetra-Substituted Fluorotyrosines: New Probes for Enzymes that Use Tyrosyl Radicals in Catalysis. *J. Am. Chem. Soc.* 2006; 128:1569–1579. [PubMed: 16448128]

- (27). Ekberg M, Birgander P, Sjöberg B-M. *In Vivo* Assay for Low-Activity Mutant Forms of *Escherichia coli* Ribonucleotide Reductase. *J. Bacteriol.* 2003; 185:1167–1173. [PubMed: 12562785]
- (28). Seyedsayamdost MR, Yee CS, Reece SY, Nocera DG, Stubbe J. pH Rate Profiles of FnY356–R2s (n = 2, 3, 4) in *Escherichia coli* Ribonucleotide Reductase: Evidence that Y356 Is a Redox-Active Amino Acid along the Radical Propagation Pathway. *J. Am. Chem. Soc.* 2006; 128:1562–1568. [PubMed: 16448127]
- (29). Zhang M-T, Hammarström L. Proton-Coupled Electron Transfer from Tryptophan: A Concerted Mechanism with Water as Proton Acceptor. *J. Am. Chem. Soc.* 2011; 133:8806–8809. [PubMed: 21500853]
- (30). Reece SY, Seyedsayamdost MR, Stubbe J, Nocera DG. Electron Transfer Reactions of Fluorotyrosyl Radicals. *J. Am. Chem. Soc.* 2006; 128:13654–13655. [PubMed: 17044670]
- (31). Gray HB, Malmstrom BG, Williams RJP. Copper Coordination in Blue Proteins. *J. Biol. Inorg. Chem.* 2000; 5:551–559. [PubMed: 11085645]
- (32). Liu J, Chakraborty S, Hosseinzadeh P, Yu Y, Tian S, Petrik I, Bhagi A, Lu Y. Metalloproteins Containing Cytochrome, Iron-Sulfur, or Copper Redox Centers. *Chem. Rev.* 2014; 114:4366–4469. [PubMed: 24758379]
- (33). Dongare P, Maji S, Hammarström L. Direct Evidence of a Tryptophan Analogue Radical Formed in a Concerted Electron–Proton Transfer Reaction in Water. *J. Am. Chem. Soc.* 2016; 138:2194–2199. [PubMed: 26871741]



**Figure 1.**

Subunit affinity ( $K_D$ ) of the  $Y_{356}W$ -photo $\beta_2$ : $\alpha_2$  complex was assessed by adding increasing amounts of  $Y_{356}W$ -photo $\beta_2$  to reaction mixtures of wt- $\alpha_2\beta_2$ , and measuring the specific activities (SAs) for each reaction. In a final volume of 300  $\mu$ L, each reaction contained 0.2  $\mu$ M wt- $\beta_2$ , 0.1  $\mu$ M wt- $\alpha_2$ ,  $Y_{356}W$ -photo $\beta_2$  (0–5  $\mu$ M), 30  $\mu$ M TR, 0.5  $\mu$ M TRR, 1 mM CDP, 3 mM ATP, 0.2 mM NADPH in assay buffer, where the absorbance decrease at 340 nm representing consumption of NADPH was used to determine SA. Data were analyzed as previously reported, to give a  $K_D$  of  $0.8 \pm 0.1$   $\mu$ M where the error bars represent 1 s.d. from duplicate measurements.

**Figure 2.**

Photophysical schemes describing the photogeneration of  $\text{W}^\bullet$  by (a) direct quenching of the excited state of the [Re] complex ( $[\text{Re}^{\text{I}*}]$ ) and (b) by the oxidized  $[\text{Re}^{\text{II}}]$  complex furnished from the flash-quench method. (c) Latimer diagram describing of the energetics relevant to the direct quenching and flash-quench pathways.



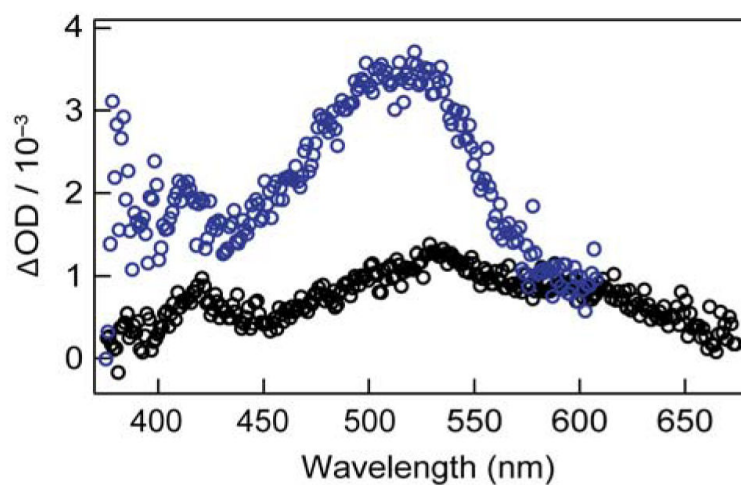


**Figure 3.**

TA spectra of Y<sub>356</sub>W- and Y<sub>356</sub>F-photo $\beta_2$  alone and in complex with  $\alpha_2$  collected 8  $\mu$ s after the 355 nm excitation pulse. The displayed spectra are averages of 3 independently prepared samples, containing either 75  $\mu$ M wt- $\alpha_2$  and 50  $\mu$ M Y<sub>356</sub>W-photo $\beta_2$  or 50  $\mu$ M wt- $\alpha_2$  and 30  $\mu$ M Y<sub>356</sub>F-photo $\beta_2$  (blue and black, respectively). Samples also contained 1 mM CDP, 3 mM ATP, and 10 mM Ru(NH<sub>3</sub>)<sub>6</sub>Cl<sub>3</sub>, in assay buffer at pH 7.6.

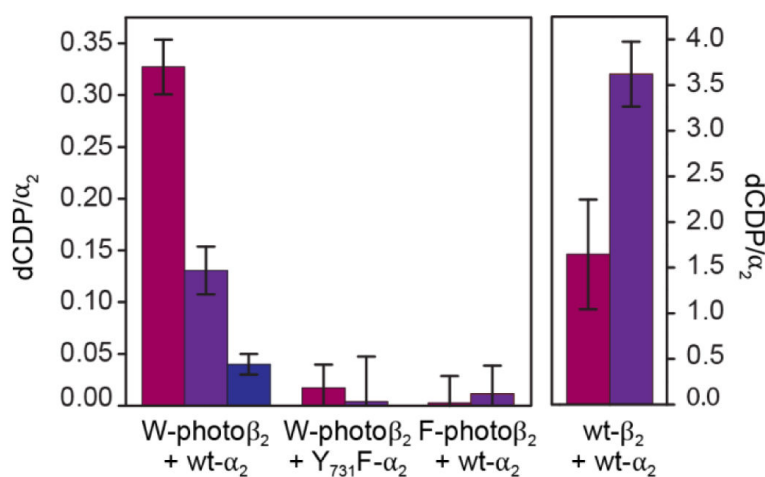


**Figure 4.**

Photochemical single turnover experiments in the presence (burgundy) and absence (purple) of 10 mM Ru(NH<sub>3</sub>)<sub>6</sub>Cl<sub>3</sub> relative to experiments performed in the dark (blue). Samples contained 10 μM or 20 μM of Y<sub>356</sub>W-photoβ<sub>2</sub>, Y<sub>356</sub>F-photoβ<sub>2</sub> or wt-β<sub>2</sub> (containing the native tyrosyl radical at 1.2 Y•/β<sub>2</sub> and lacking the [Re<sup>I</sup>] photosensitizer), and 10 μM Y<sub>731</sub>F- or wt-α<sub>2</sub> as indicated, 0.2 mM [5-<sup>3</sup>H]-CDP (26,700 cpm/nmol), and 3 mM ATP, in assay buffer at pH 7.6. Error bars represent 1 s.d. from triplicate measurements on independently prepared samples.

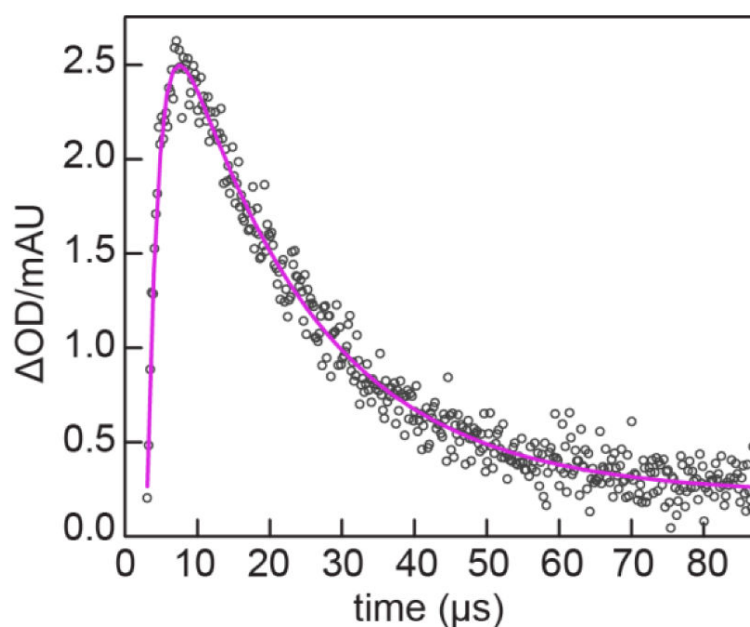


**Figure 5.**

Single wavelength TA kinetics centered at  $520 \pm 1$  nm for an average of 3 samples, each containing 50  $\mu\text{M}$   $\text{Y}_{356}\text{W}$ -photo $\beta_2$ , 75  $\mu\text{M}$  wt- $\alpha_2$ , 1 mM CDP, 3 mM ATP, 10 mM  $\text{Ru}(\text{NH}_3)_6\text{Cl}_3$ , in assay buffer at pH 7.6. The pink line is a fit of the data to Eq. 1, yielding rate constants of  $6.6 \pm 0.4 \times 10^5 \text{ s}^{-1}$  for the growth, and  $4.4 \pm 0.2 \times 10^4 \text{ s}^{-1}$  for decay of the  $\text{W}^\bullet$  signal. The growth signal is convoluted with the photo $\beta_2$  emission, and thus may not represent the actual rate of formation of  $\text{W}_{356}^\bullet$ .

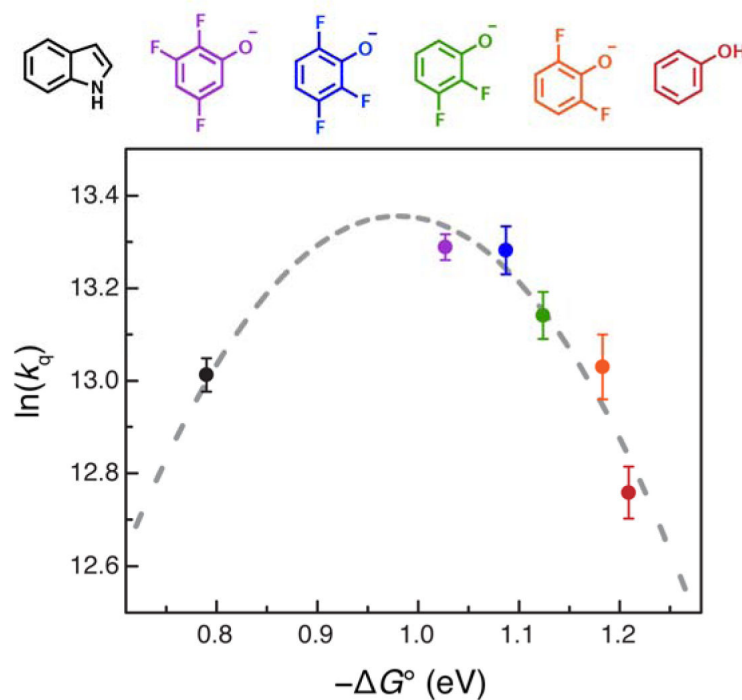


**Figure 6.**

Correlation of the natural log of  $k_q$  with  $-\Delta G^\circ$  for charge-separation within the photo $\beta_2$ : $\alpha_2$  complexes with the specified residue at position 356. Dashed lines represent simulations to the semi-classical Marcus equation (described in ref 13) with  $r = 12.5 \text{ \AA}$ ,  $\lambda = 0.98 \text{ eV}$ , and  $H_{DA} = 0.051 \text{ cm}^{-1}$ . All data except that of Y356W-photo $\beta_2$  (black, Table 1, calculated according to Eq. 3) are reproduced from ref 13. Error bars represent 1 s.d. for triplicate measurements on independently prepared samples, calculated according to Eq. 4.

**Table 1**Pathway-Dependent Excited-State Quenching at the Y<sub>356</sub>W-photoβ<sub>2</sub>:α<sub>2</sub> Subunit Interface

Interface Residues		<sup>3</sup> [Re <sup>I</sup> ]* Lifetime <sup>a</sup>	Quenching Rate Constant
β <sub>356</sub>	α <sub>731</sub>	τ / ns	k <sub>q</sub> / 10 <sup>5</sup> s <sup>-1</sup>
W	Y	549 (4)	4.4 (2)
F	Y	725 (8)	
W	F	565 (2)	4.1 (2)
F	F	733 (11)	

<sup>a</sup>Emission lifetimes measured on samples of 10 μM Y<sub>356</sub>W-photoβ<sub>2</sub> or Y<sub>356</sub>F-photoβ<sub>2</sub> and 25 μM wt-α<sub>2</sub> or Y<sub>731</sub>F-α<sub>2</sub> (as indicated), 1 mM CDP and 3 mM ATP in assay buffer at pH 7.6, λ<sub>exc</sub> = 355 nm, λ<sub>det</sub> = 600 nm. k<sub>q</sub> calculated according to Eq. 3. Representative decay traces shown in Figure S2. Error limits shown in parentheses represent 1 s.d. from triplicate measurements on independently prepared samples.